# Detection of Pedestrians in Road Environments with Mutual Interference

**C. Fischer***, **M. Barjenbruch****, **H. L. Bloecher***, **W. Menzel****

*Daimler AG, Group Research and Advanced Engineering
Wilhelm-Runge-Str., 11, 89081 Ulm, Germany
email: christoph.c.fischer@daimler.com

**Ulm University
Albert-Einstein-Allee, 41, 89069 Ulm, Germany

***Abstract:*** *In this paper the influence of mutual radar sensor interference on the detection performance of small targets, i.e. pedestrians, is investigated using simulations and measurements. For this purpose an interference model for the Chirp Sequence modulation is developed. Simulations are performed with this model and characteristic effects of this kind of interference are shown. Then the simulation results are compared to real world measurement results.*

## 1. Introduction

Pedestrian safety has been an important aspect of passive safety systems for a long time. With the ever-increasing capabilities of active driver assistance systems it is natural to implement pedestrian protection using the existing radar sensor infrastructure. The first step for implementation is the reliable detection of pedestrians, which has already received some attention in publications [1, 2]. Having a significantly smaller radar cross section than cars and bicycles, detecting pedestrians is a more demanding task. With increasing market penetration of radar-based systems, the interaction of these is coming into focus as well. This paper investigates the implication of mutual radar sensor interference on the detection performance of small targets, i.e. pedestrians.

## 2. Mechanisms of Mutual Sensor Interference

Mutual interference of radar sensors using the Frequency Modulated Continuous Wave (FMCW, [3]) waveform has been investigated in [4]. The result of crossing FMCW ramps is a spike in the time domain IF signal resulting in a wide spread noise floor increase in the range domain. This mechanism can be extended to radar sensors using the Chirp Sequence (CS) waveform. A typical CS signal considered here consists of a sequence of linear frequency ramps, each lasting $20\,\mu s$. As for the slower FMCW, the covered bandwidth depends on the targeted range resolution. FMCW frequency ramps have a significantly longer duration of at least 1 ms. Due to this difference in duration, a slow FMCW signal may cross a fast CS signal multiple times per

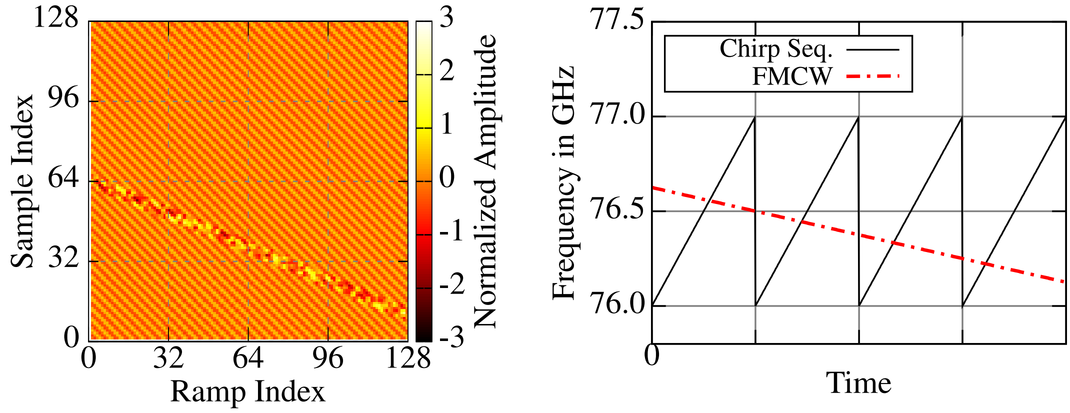


Figure 1: Simulation of the IF signal of a CS with an FMCW ramp interferer (left) and qualitative illustration of the time-dependent frequencies of the two signals (right).

CS measurement cycle as depicted in Fig. 1. During the train of chirps, the FMCW signal moves through the sweep bandwidth occupied by the CS sensor, the ramps intersecting at different times and frequencies.

In order to derive a description of received interference signal, the different receiver stages of a CS based radar sensor have to be taken into account as shown in Fig. 2.

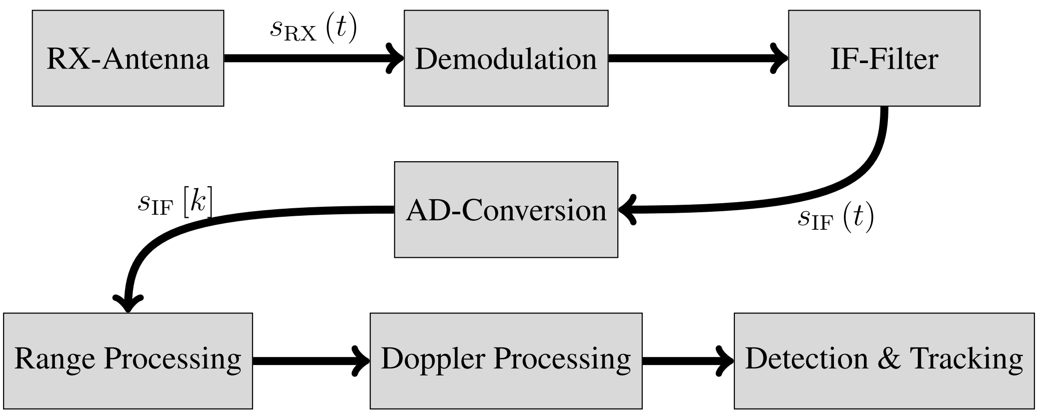


Figure 2: Basic building blocks for a generic simulation environment: The analog processing stages are drawn at the top and the digital processing stages at the bottom of the graph.

The signal processing steps before the analog digital conversion are reduced to a minimum. After reception by the antenna, assumed to be ideal here (no angular dependency of the simulated signal is introduced), the received radio frequency signal is down-converted to the baseband, filtered and sampled. This means the only analog processing steps that need to be simulated are the antenna as the signal source, and the demodulation, where the received signal $s_{\mathrm{RX}}$ is multiplied with the current transmit signal $s_{\mathrm{TX}}$ and convolved with the IF filter impulse response $h(t)$:

$$s_{\mathrm{IF}}(t) = [s_{\mathrm{RX}}(t) \cdot s_{\mathrm{TX}}(t)] * h(t) \tag{1}$$

For the most common case of a linear ramp FMCW with slope $S$, this results in an IF signal with a constant frequency that depends only on the distance $r$ of the observed target:

$$s_{\mathrm{IF}}(t) = \cos\left(4\pi\frac{r}{c}St + \varphi\right) * h(t), \tag{2}$$

with the speed of light $c$ and an additional phase term $\varphi$. When considering a target moving slowly relative to a sensor transmitting multiple FMCW ramps in sequence, this movement results in a phase shift between the individual ramps. In this context, slowly means that the target does not leave a range cell during one measurement cycle. Consequently the resulting IF signal for ramp $m$ becomes

$$s_{\mathrm{IF},m}(t) = \cos\left(4\pi\frac{r}{c}St + 4\pi\frac{v}{c}f_0(t + mT) + \varphi\right) * h(t), \tag{3}$$

with carrier frequency $f_0$ and target velocity $v$. After analog-to-digital conversion the resulting digital signal is Fourier transformed in both sample and ramp domain (corresponding to fast and slow time). This transformation yields a two dimensional matrix with cells representing range and velocity.

The model for an interference signal $s_{\mathrm{I}}(t)$ resulting from the direct over-the-air interference by the emission of another FMCW sensor (the interferer) with the slope $S_{\mathrm{I}}$ and the carrier frequency $f_{0,\mathrm{I}}$ is

$$\begin{aligned} s_{\mathrm{I}}(t) &= \cos\left(2\pi\int_0^t \Delta f(t)\,\mathrm{d}t + \varphi\right) * h(t) \quad \text{with } \Delta f(t) = (f_{0,\mathrm{V}} + S_{\mathrm{V}}t) - (f_{0,\mathrm{I}} + S_{\mathrm{I}}t) \\ &= \cos\left(2\pi(f_{0,\mathrm{V}} - f_{0,\mathrm{I}})t + \pi(S_{\mathrm{V}} - S_{\mathrm{I}})t^2 + \varphi'\right) * h(t), \end{aligned} \tag{4}$$

the function $h(t)$ being the impulse response of the interfered sensor's receive filter situated before digitization and quantization. For first considerations, a perfect bandpass filter can be assumed with cutoff frequencies $f_1$ and $f_2$ (with orders of magnitude $1\,\mathrm{MHz}$ for $f_1$ and $10\,\mathrm{MHz}$ for $f_2$). The width of the IF filters in radar sensors using CS waveforms is a major difference to the setup presented in [4, 5]. In the event of an interference, the duration is longer and therefore the observed decrease in signal to noise ratio (SNR) is expected to be proportionally large for one single ramp. For a train of $N$ ramps the resulting IF signal for the $m$th ramp is

$$s_{\mathrm{I},m}(t) = \cos\left(2\pi(f_{0,\mathrm{V}} - f_{0,\mathrm{I}} - mTS_{\mathrm{I}})t + \pi(S_{\mathrm{V}} - S_{\mathrm{I}})t^2 + \varphi'\right) * h(t) \quad m = 0 \ldots N-1. \tag{5}$$

The final input signal for further signal processing is the superpositioning of (3), (4) and additional White Gaussian Noise (WGN) $n_m(t)$

$$\begin{aligned} s_{\mathrm{IF,m}}(t) = {} & \cos\left(4\pi\frac{r}{c}S_{\mathrm{V}}t + 4\pi\frac{v}{c}f_{0,\mathrm{V}}(t + mT) + \varphi\right) * h(t) \\ & + \cos\left(2\pi(f_{0,\mathrm{V}} - f_{0,\mathrm{I}} - mTS_{\mathrm{I}})t + \pi(S_{\mathrm{V}} - S_{\mathrm{I}})t^2 + \varphi'\right) * h(t) \\ & + n_m(t). \end{aligned} \tag{6}$$

The frequency of the interference changes by the amount $TS_{\mathrm{I}}$ per ramp, making the interference signal incoherent with respect to the subsequent Doppler processing. This results in a spread of the received interference power over all Doppler cells as displayed in Fig. 3 in the following section.

## 3. Simulation Results

For the simulation of the expected effects, the signal models presented in the previous chapter have been implemented in a software environment. Three different signals were generated: The useful signal $s_\mathrm{V}[k]$ (i.e. the signal reflected off the target, according to Eq. (3)), the interference signal $s_\mathrm{I}[k]$ (according to Eq. (4)) and a WGN signal $n[k]$ to account for the different noise contributions. The superpositioned signals are fed to a 2D-FFT for range-Doppler processing. Additionally the SNR and the SIR (signal to interference ratio) are computed:

$$\mathrm{SNR_{dB}} = 10\log_{10}\frac{\sum_{m,k} s_{\mathrm{V},m}[k]\, s_{\mathrm{V},m}[k]^*}{\sum_{i,l} n_i[l]\, n_i[l]^*} \tag{7}$$

$$\mathrm{SIR_{dB}} = 10\log_{10}\frac{\sum_{m,k} s_{\mathrm{V},m}[k]\, s_{\mathrm{V},m}[k]^*}{\sum_{i,l} s_{\mathrm{I},i}[l]\, s_{\mathrm{I},i}[l]^*} \tag{8}$$

As the signal $s_\mathrm{I}[k]$ is the interference signal after the filter in the receive chain, only a fraction of the signal's power contributes to a distortion of the range-Doppler plot. This fraction $r$ can be approximated by the relation of the complete RF bandwidth of the interference signal $B_\mathrm{I}$ to twice the bandwidth of the IF filter:

$$r = \frac{2B_\mathrm{IF}}{B_\mathrm{I}} \tag{9}$$

To account for high power interference signals that drive the input stages into saturation, the complete signal power has to be considered. Other signals with amplitudes that do not affect the input amplifiers already experience significant processing gain (i.e. interference reduction) before digital processing even begins.

One exemplary result for a strong interference signal is shown in Fig. 3. The amplitude of the chosen signal is large to show the characteristic effects of the interference signal over the WGN. In the graph, an increase of the noise level by about $10\,$dB is visible. Notably the noise floor resulting from the interference signal differs significantly from the flat noise floor resulting from the WGN as shown in the upper graph, the WGN having a much smoother characteristic.

## 4. Measurement Results

For the conducted measurements, a radar sensor using the CS waveform and operating in the $76\,$GHz band was utilized. The measurement bandwidth was set to $600\,$MHz and one complete measurement cycle consisted of 128 individual ramps.

One exemplary range-Doppler measurement selected from the measurement series is shown together with the investigated scenario in Fig. 4. The time-domain characteristic of the observed interference is very similar to the simulated scenario displayed in Figs. 1 and 3. The pattern of the interference is visible in the graph. Compared to the simulation in the previous chapter the amplitude of the interference is approximately $2\,$dB relative to the noise floor of the radar sensor.

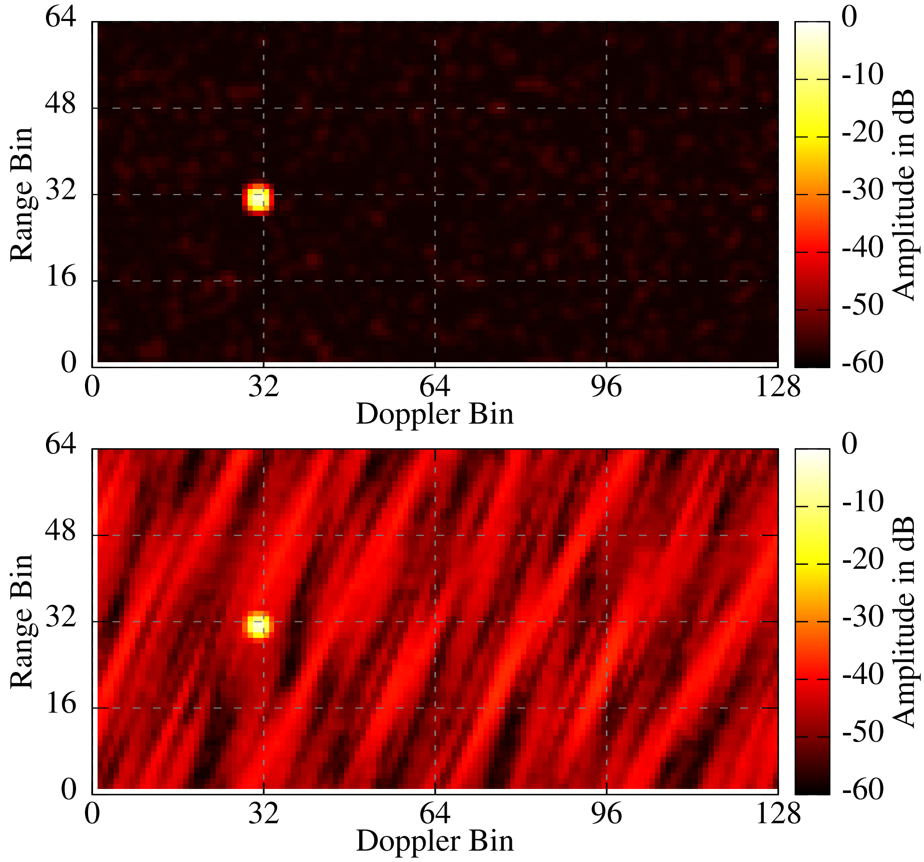


Figure 3: Simulated Range-Doppler plots of a single target using a Chirp Sequence waveform (128 ramps, 128 samples per ramp) without interference (upper graph, SNR=20 dB, SIR=$\infty$ dB) and with a strong FMCW ramp in the same band (lower graph, SNR=20 dB, SIR=18 dB), similar to the scenario in Fig. 1.

Although this has been found to be the measurement with the strongest interference impact at hand, this marginal noise floor increase is too weak to influence the detection of the pedestrian negatively.

## 5. Conclusion

In this paper the principle of FMCW versus CS interference has been investigated and key parameters for a simulation environment were presented. Additionally, the simulations have been verified by measurements using an experimental 76 GHz radar sensor. The interference effects found have shown to be clearly distinguishable from white noise or influence from clutter signals. Also the magnitude of the measured interference patterns indicates that for the investigated scenarios no negative influence is to be expected, not even for the detection of weak targets like pedestrians. Further investigations using the Norm Interferer [6] will expand the measurement catalog significantly and will help to assure the detection performance of radar sensors in as many situations as possible.

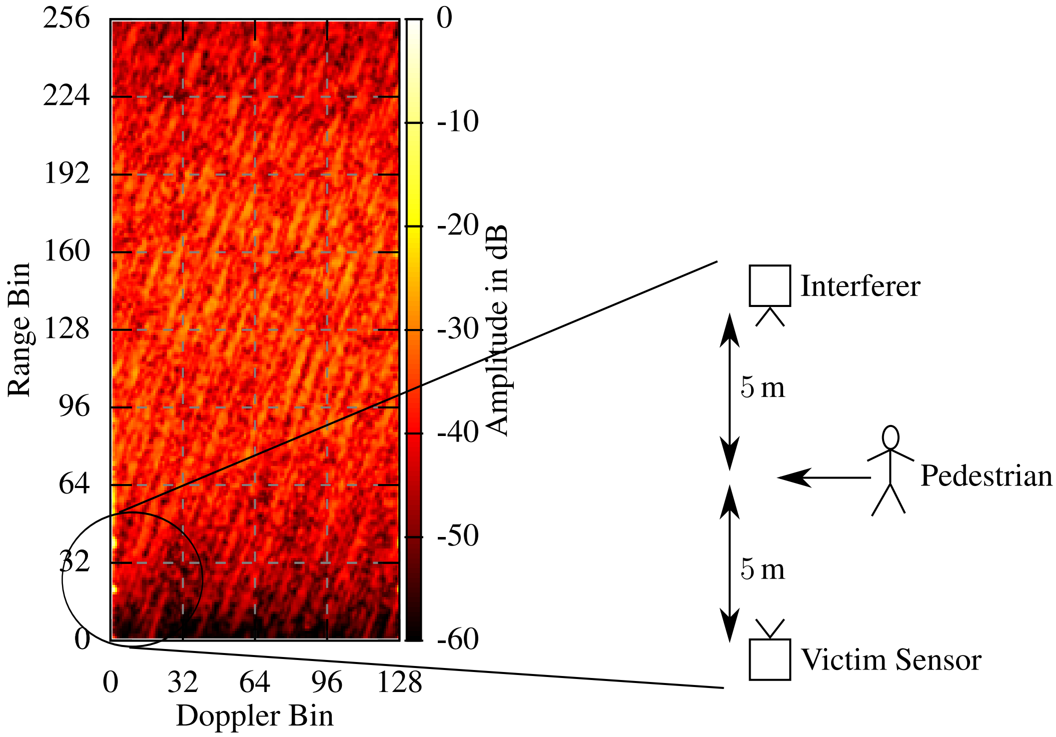


Figure 4: Range-Doppler plot of a measured scene with a sketch of the scene depicted on the right.

## 6. Acknowledgement

The research leading to these results has received funding from the European Community's Seventh Framework Programme (FP7/2007-2012) under grant agreement n° 248 231 – MOSARIM Project.

## References

[1] Henning Ritter and Hermann Rohling. Pedestrian detection based on automotive radar. In *IET International Conference on Radar Systems, 2007*, pages 1–4. IET, October 2007.

[2] A. Bartsch, F. Fitzek, and R. H. Rasshofer. Pedestrian recognition using automotive radar sensors. *Advances in Radio Science*, 10:45–55, 2012.

[3] V. Winkler. Range Doppler detection for automotive FMCW radars. In *4th European Radar Conference (EuRAD), 2007*, pages 166–169. IEEE, October 2007.

[4] Markus Goppelt, Hans-Ludwig Blöcher, and Wolfgang Menzel. Analytical investigation of mutual interference between automotive FMCW radar sensors. In *6th German Microwave Conference*, pages 312–315, March 2011.

[5] Markus Goppelt, Hans-Ludwig Blöcher, and Wolfgang Menzel. Automotive Radar – Investigation of Mutual Interference Mechanisms. *Advances in Radio Science*, 8:55–60, 2010.

[6] Felipe Torres, Christian Frank, Wolfgang Weidmann, Tobias Mahler, Tom Schipper, and Thomas Zwick. The Norm-Interferer – An universal tool to validate 24 and 77 GHz band automotive radars. In *9th European Radar Conference (EuRAD), 2012*, pages 6–9. IEEE, October 2012.